

# Novel Observer Based Force Control for Active Magnetic Bearings

Claudius M. Zingerli and Johann W. Kolar  
 Power Electronic Systems Laboratory  
 ETH Zurich  
 8092 Zurich, Switzerland  
 Email: zingerli@lem.ee.ethz.ch

**Abstract**—State of the art active magnetic bearings are controlled using a current reference, a current observer or the current as a state variable in a state-space controller. Using the current to express the state of a magnetic bearing has several disadvantages such as an unstable zero, hidden information such as stray flux, eddy currents, magnetization or hysteresis of the iron core material. Above all, it is in a nonlinear relation with both the generated force and the air gap.

In this paper a novel method is presented to directly and linearly control the force of a magnet using a force controller that is based on a flux estimator. The method is verified with simulations as well as with measurements. It decouples the magnet and position controllers, eases the modeling of non-ideal parameters of magnetic bearings, reduces noise, has a larger range of displacement and behaves intrinsically linear.

**Index Terms**—Magnetic levitation, Force control, Observer, Modeling, Eddy currents, Magnetic Hysteresis, Stray flux

## I. INTRODUCTION

Active Magnetic Bearings (AMBs) are a popular choice in high-speed rotating machines. They allow virtually loss-free, contact-less and maintenance-free operation, and are accordingly often used in turbo machinery, high-speed grinding or blowers [1]. They allow vibration control, active damping, exact or fine positioning and monitoring of the levitated part. Their main disadvantages of AMBs are the limited load capacity (35 N per cm<sup>2</sup> pole area according to [1]), the need for an electric power supply and increased complexity compared to alternatives such as bush or ball bearings [2].

Active magnetic bearings include an actively controlled element which usually consists of one or more electromagnets.

This paper explains the current state of the art in Active Magnetic Bearings and its problems. It proposes a novel control method to overcome these problems - by making use of a force controller - an approach that has been verified both in simulation and through experiments.

## II. STATE OF THE ART AMB CONTROLLER

Presently most AMBs use a current amplifier with current feedback to supply the magnets [3]. By using such a current-controlled amplifier, the generated force becomes a function

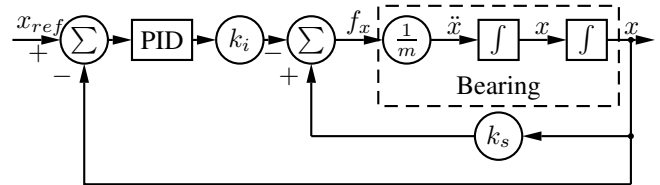


Fig. 1. State of the art current-controlled magnetic bearing [6].

of the rotor position and is nonlinearly coupled to the current

$$F = \frac{A_{fe} \cdot \mu_0 \cdot N^2}{4} \cdot \frac{I^2}{x^2} \quad (1)$$

where  $A_{fe}$  is the pole area,  $N$  the number of turns and  $x$  the total air gap. The air gap  $x$  in the denominator induces a negative stiffness that has to be compensated - usually with a cascaded position controller.

A typical linearized implementation of such a controller is shown in Figure 1 which implements the equation:

$$F = k_i \cdot I + k_s \cdot x \quad (2)$$

where  $k_i$  and  $k_s$  are the current and position gradients in the desired operating point [4].

The dependency of the air gap  $x$  results in a transfer function that is a function of the rotor position, the dependency of the current  $I$  makes the transfer function dependent on the external load. Both dependencies make a proof of stability under all operating conditions - which is often mandatory, difficult and rather complex.

Being able to change the rotor position allows for optimization of the angle of attack in a turbo machine, so as to optimize efficiency and compensate for thermal expansion. Independence of the external load facilitates the commissioning and tuning of the position controller, and thus compensates for rotor dynamic aspects.

In real-world magnetic bearing systems, the position controller's order may be well above 100 states in order to account for all degrees of freedom, effects of drag, couplings, eigenfrequencies of the foundation, chassis, machine, rotor, and blades. Hence, if the bearing and its controller could

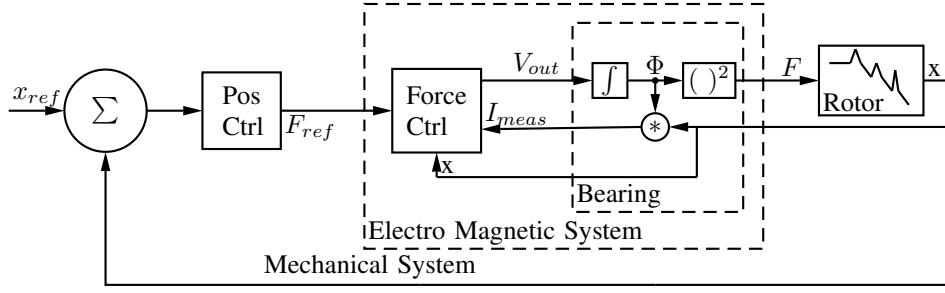


Fig. 2. Proposed novel observer based force control

be considered as a linear force amplifier as shown in Figure 2, the the design of the position controller would be greatly facilitated.

In practical implementations of current-controlled magnetic bearings usually a second bearing on the opposite side of the rotor/thrust disc is added and a bias current is flowing through both of them (usually  $I_{bias} = 40...50\% I_{max}$  according to [5]). This differential connection linearizes the force-current dependency in a limited range, but not the force-position dependency.

Indeed, a bias current boosts the transient response, but it also creates significant losses. Several publications address this problem and propose theoretical solutions to minimize necessary bias current, but drop the concept of a cascaded controller (e.g. [3], [5]).

A cascaded controller decouples the now completely *mechanic* position controller and *magnetic* power amplifier controller and therefore eases design and commissioning of an AMB system. It allows decentralized and redundant controllers which is why we want to keep the cascaded approach.

### III. NOVEL FORCE CONTROLLER

#### A. Basic Idea

Assuming a steady state followed by a small disturbance in the rotor moving away from the bearing core, the flux stays constant, but as the air gap increases, the inductivity decreases. The current instantly raises and the current controller outputs a negative voltage, trying to reduce the current. This negative voltage reduces the flux and thereby also the force, which is why the rotor moves further away.

This instability is usually compensated for by the position controller that changes its force reference to a higher value. That is why making the (inner) current control loop faster than the outer position control loop could even destabilize the system.

#### B. Mathematical model

With the following analytical investigation of the magnetic bearing, the generated force  $F$  is determined as a function of the voltage  $V_w$  applied to the bearing. The basic idea is similar to methods used in modeling of electrical machines for direct torque control controllers as described in [7], where

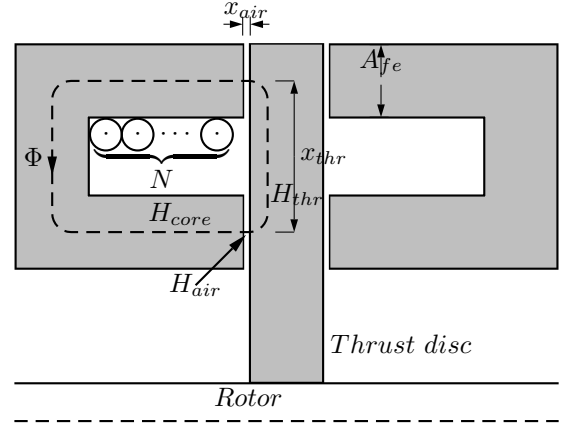


Fig. 3. Geometric model

a rotating flux is controlled in contrary to a movable rotor in the magnetic bearing.

Using Maxwell's equations for the magnetic field strength  $H$  leads to

$$\sum_{\forall i} I_i = \oint_S \vec{H} \cdot d\vec{s}$$

$$N \cdot I = \underbrace{2 \cdot x_{air} \cdot H_{air}}_{I_{air}} + \underbrace{x_{core} \cdot H_{core}}_{I_{core}} + \underbrace{x_{thr} \cdot H_{thr}}_{I_{thr}} \quad (3)$$

where  $N$  is the number of turns,  $x_{air}$ ,  $x_{core}$  and  $x_{thr}$  the mean-field line length in the according part (see Figure (3)).

The integral in (3) is split in core, thrust disc and air gap parts. The force generated in the air gap is of interest. Assuming a constant field density  $\Phi/A_{fe}$  over the entire pole area  $A_{fe}$  leads to

$$I_{air} = \frac{2 \cdot x_{air}}{N} \cdot H_{air} = \frac{2 \cdot x_{air}}{N \cdot \mu_0 \cdot A_{fe}} \cdot \Phi \quad (4)$$

The magnetic energy  $W$  in the air gap is determined using (4) and Faraday's law of induction

$$W = \int v(t) \cdot i(t) dt \Big|_{v(t)=\frac{d}{dt}\Phi \cdot N, i(t)=I_{air}}$$

$$= \frac{x_{air}}{\mu_0 \cdot A_{fe}} \cdot \Phi^2 \quad (5)$$

Thus the mechanical force is calculated to

$$F = \frac{W}{x} = \frac{1}{\mu_0 \cdot A_{fe}} \cdot \Phi^2 \quad (6)$$

Consequently, the voltage  $V_w$  required in order to generate the force  $F$  is

$$\Phi = \frac{1}{N} \cdot \int V dt$$

$$V_w = N \cdot \sqrt{\mu_0 \cdot A_{fe}} \cdot \frac{d}{dt} \sqrt{F} \quad (7)$$

(7) provides a method to calculate the bearing force  $F$  by integrating the applied voltage  $V_w$ , or vice-versa to calculate the voltage-time-area required for a desired force. Compared to a current-controlled bearing, there is no need to compensate for the varying air gap. This method is intrinsically used in flux or voltage controlled magnetic bearings. The difference is that in the control method presented in this paper, the magnetic flux (or flux density) is used as a state so as to easily model nonideal parameters explained in the following.

In practice, several effects cause the estimation of the flux (i.e. the integration of the voltage) to be too inaccurate:

- Inaccuracy of the PWM duty cycle
- Ohmic losses in cables, bearing coils, amplifier' output impedance
- Forward voltages and dead times of the amplifier
- Eddy currents
- Stray flux
- Electrical and magnetic coupling between channels/axes

Therefore, in previous literature (e.g. [6], [8]) the magnetic flux  $\Phi_{est}$  is measured using a flux detector e.g. hall sensors, or an additional sensor coil in parallel to the bearing coil [10]. However, this approach has several disadvantages:

- Increased cabling efforts
- Additional devices in the bearing that might cause the bearing to fail. The bearing might be very difficult to service, have costly down-time and furthermore has often has to operate in a very harsh environment.
- Measuring flux induces additional dead time, provoking increased phase loss and allowing no feed-forward control.

On the contrarily, in the method presented in this paper, the current  $I_{obs}$  generated by the estimated flux  $\Phi_{est}$  is observed.  $I_{obs}$  is then compared to the amplifier's measured current  $I_{meas}$  and fed back to the flux integrator via a gain  $K$ . The proposed implementation of this observer is shown in Figure 5. Figure 4 shows an overview of the whole force controller.

In order to be able to observe the current  $I_{obs}$ , an electromagnetic model of the bearing is needed. The current observer model mainly consists of the four current-generating blocks presented in Table I.

The models must only be exact at lower frequencies, because at frequencies above the observer's pole (which is

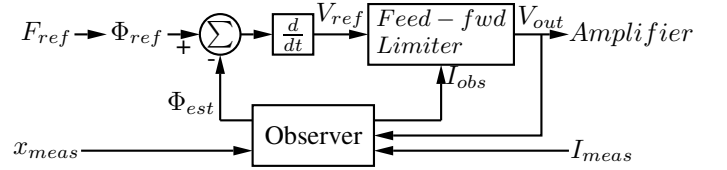


Fig. 4. Force controller internals

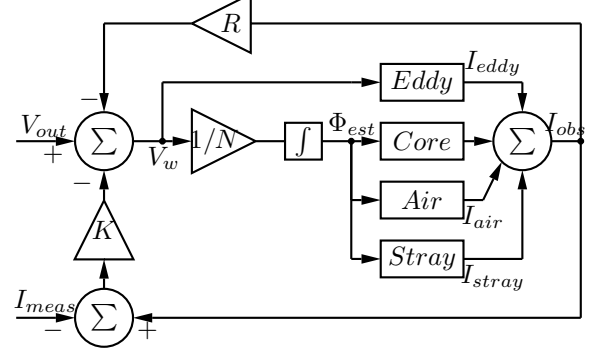


Fig. 5. Proposed observer model for one bearing.

basically a low pass filter), solely the forward path shown in Figure 4 influences the output voltage.

### C. Eddy currents

As eddy currents increase with frequency, they could put a second current limit on the amplifier, besides the well known voltage limit that confine the bearing's dynamics at higher frequencies as shown in [9]. Eddy currents may lead to local saturation and therefore reduce the effective magnetic material thickness. Having a model for eddy current allows to compensate or at least monitor their effects.

As shown in [12] and verified by measurements, eddy currents behave like a frequency-dependent impedance

$$Z_{eddy}(j\omega) = C_1 \cdot \sqrt{j\omega} \cdot \tanh(C_2 \cdot \sqrt{j\omega}) \quad (8)$$

which could be expanded to

$$Z_{eddy}(j\omega) \propto \sqrt{j\omega} \cdot \tanh \sqrt{j\omega} = \frac{j\omega}{1 + \frac{j\omega}{3 + \frac{j\omega}{5 + \frac{j\omega}{7 + \dots}}}} \quad (9)$$

TABLE I  
CURRENT-GENERATING BLOCKS IN THE OBSERVER

Block	Variable	Description
<i>Eddy</i>	$I_{eddy}$	Eddy currents induced by changing fields in bearing and thrust disc
<i>Core</i>	$I_{core}$	Current induced by magnetization of the core material
<i>Air</i>	$I_{air}$	Current induced by in the air gap
<i>Stray</i>	$I_{stray}$	Currents induced because of stray flux

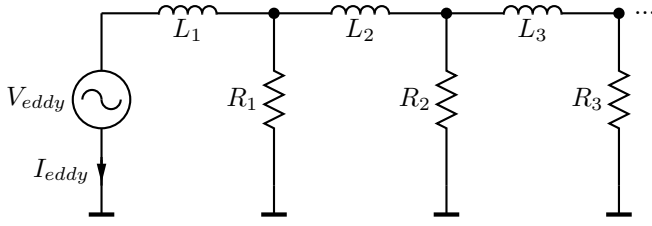


Fig. 6. Model to calculate eddy currents.

which has the form of the impedance of linked R-L elements as shown in Figure 6, leading to a magnitude that rises by 10 dB/dec and has a phase of  $60^\circ$ . This structure was used to match the measured frequency-impedance curve and was implemented in software. The number of R-L elements depends on the required precision as well as on the frequency range. In the experimental bearing (Section IV), two R-L elements approximate the measured impedance data with 1.37% average error considering phase and magnitude between 25 Hz and 200 Hz.

#### D. Core and thrust disk magnetization

To estimate the current induced by the magnetic field  $H$  in the core, its magnetization behavior needs to be known. In literature linear core models are often used (meaning linearizing the core material using a relative permeability  $\mu_r$ ). It is important to have a model that complies with the varying relative permeability  $\mu_r$  for those materials showing a soft saturation behavior such as many ferrites as well as being able to use the core material up to saturation (and beyond).

In order to account the non-linear behavior of most ferromagnetic materials, the magnetization models of Rayleigh [13], Karlqvist [14], Rivas [15] and Takacs [16] were compared to material data employing a Downhill-Simplex function to minimize the weighted error sum of squares. The resulting magnetization curves for M330-35 core material are shown in Figure 7. Rivas' model

$$B(H) = \mu_0 \cdot \left( H + \frac{a_0 + a_1 \cdot H + a_2 \cdot H^2}{1 + b_0 \cdot H + b_1 \cdot H^2} \right) \quad (10)$$

has shown the best agreement and is currently used. It's polynomial structure allows for an efficient implementation. The model was inverted to extract the current  $I_{core}$  which is proportional to the magnetic field  $H$ .

To obtain the most linear bearing force transfer function, the individual reference points were weighted proportional to  $H^2$  because the generated force is approximately proportional to the squared current.

#### E. Stray

Since at higher flux densities a significant part of the flux is stray flux that does not add to the generated force, a stray flux model has been developed which uses a magnetic circuit, as shown in Figure 8. The magnetic resistance of the core is separated in a part  $a \cdot R_{fe}$  that's being flown through by the

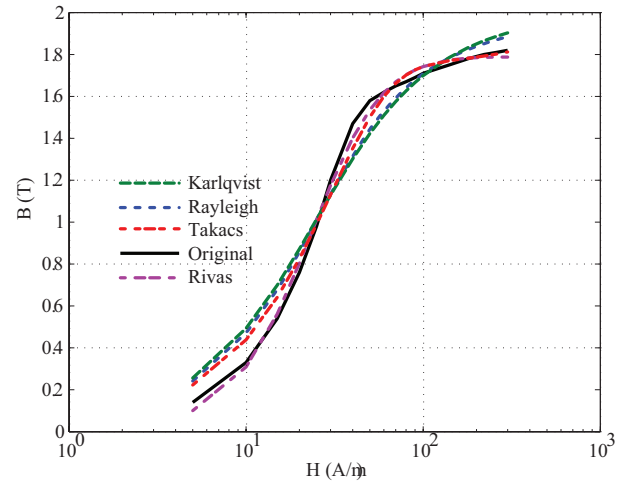


Fig. 7. Analyzed magnetization models approximating the magnetization curve of M330-35 iron.

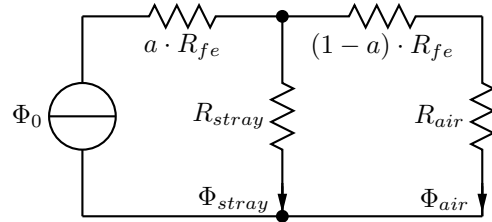


Fig. 8. Model to calculate the stray flux. Only one part of the original flux  $\Phi_0$ , that is the flux in the air gap  $\Phi_{air}$ , is generating a force to control the rotor.

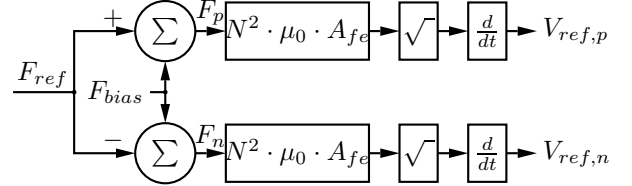


Fig. 9. Control model using force bias

original flux  $\Phi_0$  and a part  $(1-a) \cdot R_{fe}$  in which only the air gap flux  $\Phi_{air}$  flows. The difference is the stray flux  $\Phi_{stray}$  which flows through the equivalent stray resistance  $R_{stray}$ . The parameter  $a$  has been obtained from the mechanical construction of the bearing as well as the materials used.

#### F. Bias

In a force controlled differential magnetic bearing, no bias is necessary to stabilize or linearize the system, but as the voltage of the amplifier is limited, a bias increases the dynamic response for large signals. A bias can equally be achieved by a force or by a flux density as shown in Figures 9 and 10. A bias force is more descriptive in the mechanical design, whereas it is more efficient to implement a bias flux density in a model, why a flux density bias has been chosen.

As long as the dynamic requirements are achievable, bias should be minimized to minimize load on the electrical and mechanic system as well as to minimize losses.

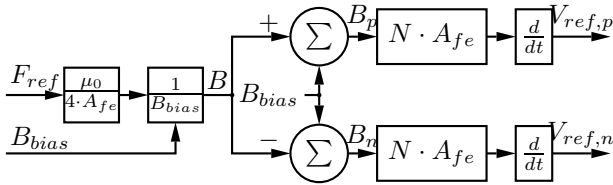


Fig. 10. Control model using magnetic bias

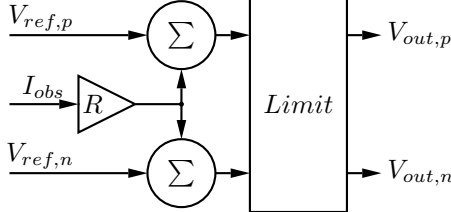


Fig. 11. Feed forward paths

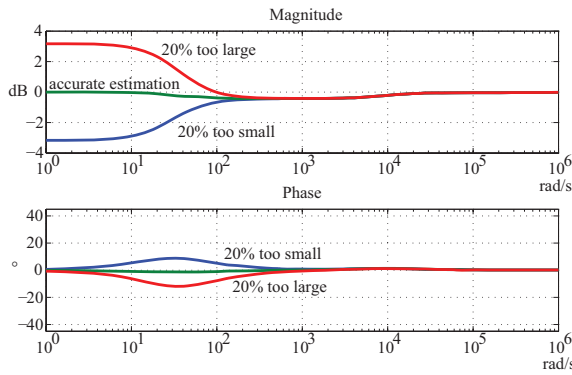


Fig. 12. Simulated force transfer function of the force controller with  $\pm 20\%$  resistance variation in the feed forward compensation (discretization and dead times are neglected)

### G. Resistance and Compensation

In contrast to a current-controlled bearing, the resistance of the system (coil, cable, amplifier) needs active compensation. This is realized by means of a feedback in the observer (Figure 5) and a feed-forward in the voltage control of the amplifier (Figure 11).

To compensate for the resistance, the observed as well as the measured current may be used. When using the observed current, the bearing model must already be a close approximation of reality or else a high observer feedback gain  $K$  is necessary.

It has proven more effective to use the observed current as the compensator's input for various reasons: less sensor noise and less dead time and, as a result, less phase loss.

In the feed-forward path, an inaccurate resistance is not compensated for by a high  $K$  and at low frequencies a force deviation would result as shown in Figure 12.

To achieve independence of the copper resistance, an adaptive resistance estimator was implemented. The resistance is estimated by integrating the product of the voltage  $V_{ref}$  times current on each bearing coil and using this *energy* as the resistance  $R$  in the compensator (Figure 11). Using the product

instead of the voltage has the advantage of increasing the integration speed at higher magnitudes, where a deviation would entail larger consequences.

The basic idea is to minimize the active power seen by the controller as, assuming that the resistance is ideally compensated, from the point of view of the controller, there is only reactive power in the bearing coil. Hysteresis and eddy currents also consume active power, but they are AC-only effects, accordingly there is a low-pass filter before the integration. The bandwidth of the filter could be as low as in the range of the thermal time constant of the bearing.

Furthermore this compensation allows to estimate the coil temperature change. If a cable with four conductors (for two differential bearings) is used to connect the amplifier and the bearing, the estimate would be an average of bearing coil and cable temperature. If a cable with three conductors is used instead, bearing coil and cable temperature can be separated. Early experiments have shown that this temperature estimation method works, but coupling between the channels and forward voltages in the amplifier needed compensation. It was possible to estimate the temperature in the order of  $\pm 10^\circ C$ .

With a similar adaptive method, that is through integration of the output voltages reduced by the ohmic and coupling losses, it has been tried to neutralize forward voltages. In a stationary environment the voltage drop caused by forward voltages is not separable from the voltage drop caused by ohmic losses and therefore enabling both methods at the same time could lead to invalid results. It is recommended to keep the less temperature sensitive value constant. Under dynamic loads to the bearing, both causes are easily distinguishable allowing adaption to both causes of voltage drop.

## IV. EXPERIMENTAL SETUP

### A. System

The proposed controller has been implemented on an existing active magnetic bearing system shown in Figure 13. The bearing is designed for a 400 kW turbo expander used to harvest energy from the pressure difference between high and low pressure natural gas pipelines instead of wasting it by using a reduction valve. Table II shows some key data and Figure 14 shows an overview of the bearing system.

All radial axes of the bearing are still controlled via the existing current controller. The axial position controller's output signals are synchronously transmitted to the new force controller implemented on a separate microcontroller and amplifier. The amplifier's PWM signals are synchronized to the controller frequency using a digital PLL to minimize time delays for voltage and current measurements.

The axial bearing has been chosen because it is made of massive, non laminated material, for the realization of which a trade-off between mechanical and magnetic properties had to be made, so large eddy currents are expected.



Fig. 13. Experimental bearing. The novel controller controls the attached axial bearing on the very left.

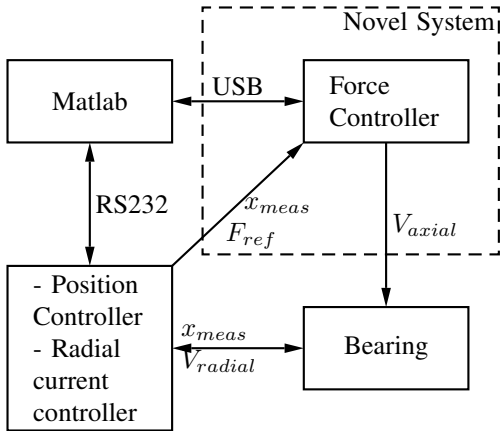


Fig. 14. Experimental setup showing the novel system in the dashed box.

Later experiments proved that it is feasible to control all axes of the bearing with a force controller. With this setup, the novel force controller is compared with the state-of-the-art current controller.

### B. Amplifier

An existing PWM three phase high-speed motor drive was used to operate the experimental bearing. The two bearing coils were connected between two phases each. This setup provokes an electrical coupling between the channels that must be taken into account. The coupling consists of four aspects:

TABLE II  
PARAMETERS OF THE EXPERIMENTAL AXIAL BEARING

Parameter	Value
Nominal air gap	$x_0 = 0.5 \text{ mm}$
Winding resistance	$R_w = 2.5 \Omega$
Rotor mass	$m = 110 \text{ kg}$
Total pole area	$A_{fe} = 75 \text{ cm}^2$
Maximum force	$F_{max} = 5 \text{ kN}$
Maximum voltage	$V_{max} = 600 \text{ V}$

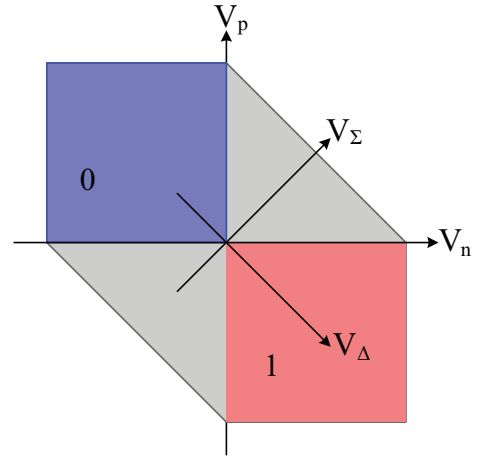


Fig. 15. Example of switching loss minimization for the common leg.  $V_p$  and  $V_n$  are the bearing voltages and  $V_\Sigma$  and  $V_\Delta$  the sum and differential voltages at the bearing coils. For bearing voltages in the blue upper left quadrant, the duty cycle of the common leg is zero, while in the red lower right quadrant the duty cycle of the common leg is one, therefore no switching losses exist. In the other areas, the common leg exhibits switching losses. Equivalent areas exist for the other two legs.

- Resistive: DC link and IGBT resistance, Cable resistance (when using a three wire cable)
- Forward voltage: IGBT and diode forward voltage
- Voltage-time area loss because of the bridge's dead times
- Duty cycle limits

If there is an output filter, depending on the configuration, there is an additional connection between channels which would influence the channel coupling.

Depending on the sign of the current in the common leg - which is equal to the difference of the two bearing currents - resistive (semiconductor resistance) and voltage (semiconductor forward/saturation voltage) couplings need to be added to or removed from the other two legs.

The limited DC link voltage limits the possible bearing voltages which has to be taken account of in the observer. By sharing a common leg, an additional restraint on achievable voltages is added. To minimize the influence of this restriction and to achieve the maximum dynamic netto force, the voltage signs are chosen in order that the differential voltage in both legs can be maximized. The common leg is thus the negative pole of the top bearing and the positive pole of the bottom bearing.

Under certain circumstances, the additional degree of freedom attained by using three duty cycles to control two voltages, allows for different strategies to reduce switching losses (through clamping one phase at a full or zero duty cycle, as shown for the common leg in Figure 15), or to equalize the different semiconductor loads (by keeping duty cycles averaged, for example with a weight proportional to the phase load).

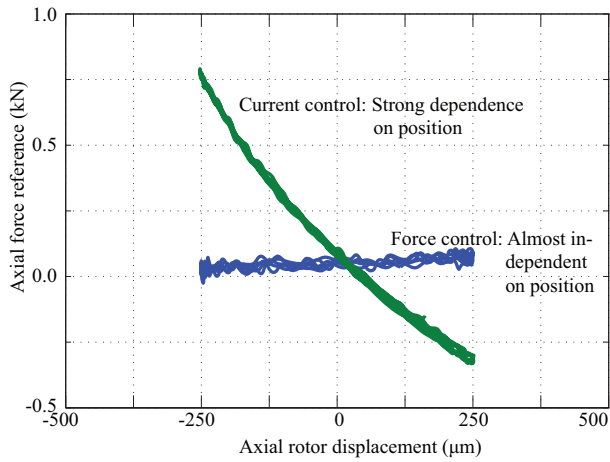


Fig. 16. Comparison force vs. current control for small amplitudes

## V. MEASUREMENTS

### A. Independence on rotor position

The rotor was moved with a sinusoidal position reference with a frequency of 1 Hz and an amplitude of  $250 \mu\text{m}$ . The output signals of the position controller (i.e. current/force reference) are shown in Figure 16, displaying the force reference on the vertical axis and the rotor position on the horizontal axis.

Since the current controller needed a bias current of about 2 A, a bias flux density of 300 mT which generates the same current was used in the force controller. If there was no bias flux at all, the comparison would be unfair for the current controller as the force controller does not need to generate a significant force, because the bias generates already 315 N while the dynamic force necessary to move the rotor is in the range of 1 N. Moreover, no external load was applied.

Magnetic bearings usually have additional retainer bearings to carry the rotor in case of overload or failure of the magnetic bearing. To test recovery from a touchdown to the retainer bearing, the excitation amplitude was increased so the rotor slightly touched the retainer bearing at about  $\pm 400 \mu\text{m}$ . The current controller had more problems to restabilize after touching as shown in Figure 17. (The journal bearing was later moved further outside to allow larger rotor displacements.)

### B. Linearity of generated force

The force and current controllers were compared at various external loads  $F_{ext}$ . The external load is made of a precision spring scale connected to a block and tackle multiplying the force by a factor of five. Figure 18 shows the behavior of the force controller at an increasing load in steps of 250 N, up to 2.75 kN. Larger loads were not tried as the limit of the burden was reached.

At higher loads the position vs. force line bends. The reasons for this are the nonlinear position sensor (about 6% deviation from the best fit linear scale) and the insufficient

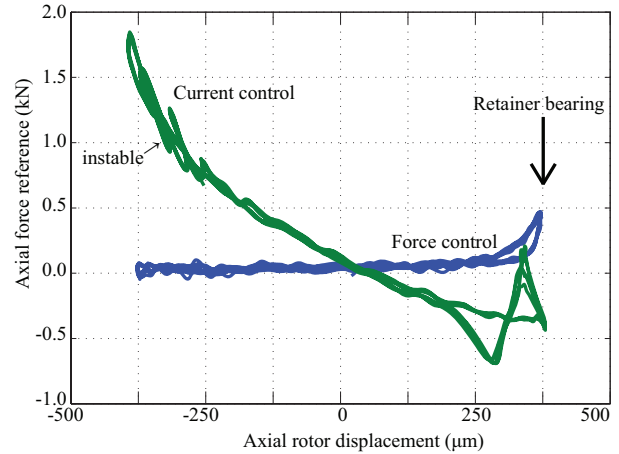


Fig. 17. Comparison force vs. current control for large amplitudes

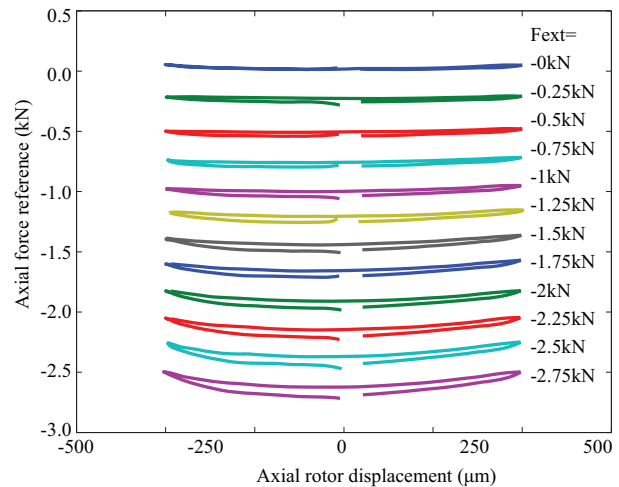


Fig. 18. Force vs. position at various external forces using the force controller

accuracy of the stray flux model. The later was examined with better analytical model.

The same experiment with the current controller is shown in Figure 19. The current controller was not able to levitate the rotor at an external force larger than  $F_{ext} = -1.75 \text{ kN}$ . The rotor stuck at the retainer bearing.

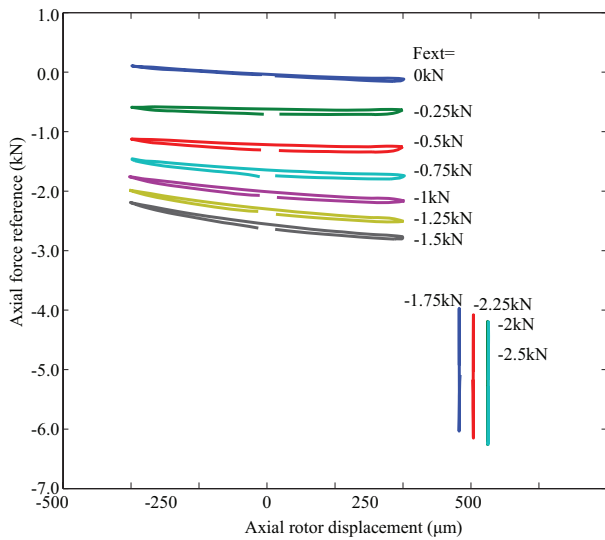


Fig. 19. Force vs. Position at various external forces  $F_{ext}$  using the current controller

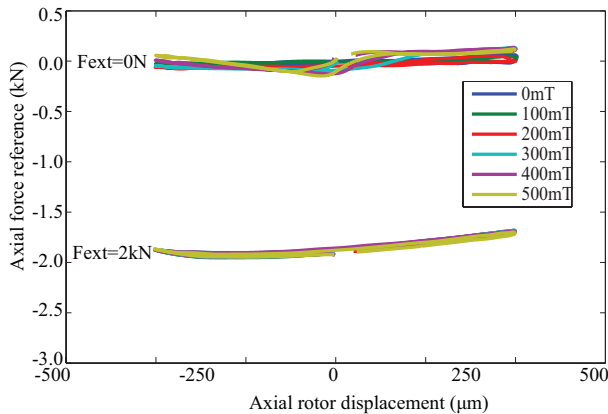


Fig. 20. Force vs. Position at various bias flux densities

### C. Independence of bias flux

The measurement in Figure 20 shows a welcome side-effect of the applied control method: There is no need for a bias flux to linearize or stabilize the system, neither does a bias flux influence the force controller.

A motivation for having some bias flux is to increase the transient response - in case there is a voltage limitation - which is usually applies. If there was no bias flux, the static losses would be minimized, but the  $dF/dt$  would initially be zero as well.

## VI. CONCLUSIONS

In this paper the development of a novel force controller for an active magnetic bearing is described to allow linear and decoupled control of an active magnetic bearing. This approach decouples the electro-magnetic and mechanic subsystems easing the design of both. The force controller has shown superior behavior compared to prevalent current controllers,

especially at large position deviations. By optionally taking account of effects like stray flux, core magnetization, eddy currents and resistance change, it enables higher utilization of existing materials without any changes in the electrical or mechanical construction. As published control method does not depend on bias flux, static losses are reduced therefore being more environmentally friendly. The observed effects allow better monitoring of the bearing parameters and state permitting early detection of aging or failures.

Compared to existing controllers the number of degrees of freedom and modeling effort is increased. But by removing the instable pole of current controllers, the robustness is increased therefore allowing a rougher parametrization of the force controller.

To our knowledge this is the first practical implementation of a force controlled active magnetic bearing.

## REFERENCES

- [1] G. Schweitzer, *Active magnetic bearings - chances and limitations*, Proc. Sixth Internat. IFToMM Conf. on Rotor Dynamics, Sydney, 2002.
- [2] P. Imoberdorf, C. Zwysig, S. D. Round and J. W. Kolar, *Combined Radial-Axial Magnetic Bearing for a 1 kW, 500,000 rpm Permanent Magnet Machine*, Applied Power Electronics Conference, APEC 2007 - Twenty Second Annual IEEE, 2007.
- [3] P. Bühler, R. Siegwart, R. Herzog *Digital Control for Low Cost Industrial AMB Applications*, Proc. Fifth Internat. Symposium on Magnetic Bearings, Kanazawa, Japan, 1996.
- [4] R. Schoeb, *Theorie und Praxis der Magnetlagertechnik*, Lecture notes, ETH Zurich, Switzerland, 2009.
- [5] P. Tsiotras and M. Arcak, *Low-Bias Control of AMB Subject to Voltage Saturation: State-Feedback and Observer Designs*, Proc. of the 41st IEEE Conference on Decision and Control, Las Vegas, Dec. 2002.
- [6] G. Schweitzer and E. H. Maslen, *Magnetic Bearings: Theory, Design and Application to Rotating Machinery*, Heidelberg, Germany: Springer, 2009.
- [7] T. J. Vyncke, R. K. Boel and J. A. A. Melkebeek, *A Comparison of Stator Flux Linkage Estimators for a Direct Torque Controlled PMSM Drive*, Proc. of the 35th IECON, Portugal, Nov. 2009.
- [8] D. Vischer, *Sensorlose und spannungsgesteuerte Magnetlager*, PhD thesis, Institute of Robotics, ETH Zurich, Switzerland, 1988.
- [9] E. E. Swanson, E. H. Maslen, G. Li and C. H. Cloud, *Rotordynamic Design Audits of AMB Supported Machinery*, Proc. 37<sup>th</sup> Turbomachinery Symposium, 2008.
- [10] S. Hara, T. Namerikawa, F. Matsumura, *Improvement of Dynamic Response by Flux Feedback on Active Magnetic Bearings*, Proc. Fifth Internat. Symposium on Magnetic Bearings, Kanazawa, Japan, 1996.
- [11] L. Kucera and M. Ahrens, *A model for axial magnetic bearings including eddy currents*, 3<sup>rd</sup> Intl. Symposium on Magnetic Suspension Technology, 1996.
- [12] R. Amstad, *Self-sensing Active Magnetic Bearing*, M. S. thesis, Laboratoire d'Automatique, EPFL, Lausanne, Switzerland, 2008.
- [13] Lord Rayleigh, *The behaviour of iron and steel under the operation of feeble magnetic force*, 23<sup>th</sup> Phil. Mag., 1887
- [14] O. Karlqvist, *Calculation of the magnetic field*, 86<sup>th</sup> Transactions of the Royal Institute of Technology, 1954
- [15] J. Rivas, J. M. Zamarro, E. Martin, C. Pereira, *Simple Approximation for Magnetization Curves and Hysteresis Loops*, IEEE Transactions on Magnetics, Vol. 17. Nr. 4, 1981
- [16] J. Takacs, *A phenomenological mathematical model of hysteresis*, COMPEL, Vol. 20. Nr. 4, 1999
- [17] J. A. Nelder and R. Mead, *A simplex method for function minimization*, The Computer Journal Vol. 7, Nr. 4, 1965